

Influence of the cut-off magnitude

Our analysis counts earthquakes with $m \geq 4.0$, without any apparent care to the fact that $m=4.0$ is below the magnitude of completeness m_c estimated to 5.0 when aggregating all sequences (cf Figure S1). Changes in m_c , in particular a decrease as time goes on and better coverage is reached by regional seismic networks, could contribute to the observed correlation between precursory acceleration and the number of aftershocks. Indeed, increasing m_c implies lowering the probability p that precursory acceleration is significant, as some foreshocks can then be removed from the dataset. We here investigate whether counting earthquakes below m_c has an impact on our analysis.

The earthquake data spans 33 years of activity, over the whole world. Variability of the magnitude of completeness m_c is thus expected from one sequence to the next. The analysis considers the earthquakes within 50 km and ± 1 year of the mainshock ; the number of these earthquakes is often small for any particular sequence, preventing us from making a thorough determination of m_c for each sequence. We thus estimate m_c as follows:

- we consider all $m \geq 4.0$ earthquakes within 50 km and ± 1 year of the mainshock.
- If there are fewer than n_{\min} such earthquakes, we extend the radius of the circular zone until we have at least n_{\min} earthquakes.
- We fit the magnitude – frequency law of the obtained subset with a Gutenberg-Richter law modulated by a probability of detection. The latter is taken to be the error function [Ogata and Katsura, 1993], which is known to provide good fits. We constrain the parameters to be within the intervals $0.7 < b < 1.3$, $4 < m < 6$ and $0.1 < \sigma < 0.5$, to avoid unrealistic solutions that sometimes occur at low numbers n_{\min} . Completeness is then defined as $m_c = m + \sigma$.

We show in Figure S2 that m_c stabilizes after 1995, when using both $n_{\min}=100$ and $n_{\min}=200$; 90% of the sequences occurring from 1995 onwards are characterized by $m_c < 4.6$. We thus run the analysis of Figure 2 to the subset of mainshocks occurring from 1995 onwards, only keeping $m \geq 4.6$

earthquakes for computing the probability of acceleration p and for the stacked number of earthquakes within 50 km and ± 1 year of the mainshock. The results in Figure S3 again display a clear correlation between the presence of a precursory acceleration and the number of aftershocks, proving that counting earthquakes below the local magnitude of completeness has no impact on this observation.

Significance of the correlation between precursory acceleration and the number of aftershocks

We check whether the mean number of aftershocks in population A really depends on the existence of precursory acceleration. To do so, we explore other intervals of p for defining population A, and measure the difference in aftershock productivity between the two populations.

Two end-case models can be considered when explaining aftershock productivity :

- (1) the number of aftershocks only depend on the magnitude of the mainshock, independently of the background rate of earthquakes. This is the key hypothesis of linear models like ETAS [Ogata, 1988] or MISD [Marsan and Lengliné, 2008].
- (2) the number of aftershocks depend on the magnitude of the mainshock, and is proportionnal to the background rate of earthquakes, as for example with the rate-and-state friction model [Dieterich, 1994].

To account for these two models, we define two measures of aftershock productivity :

- $\rho_1 = \frac{(N_A - rF_A)/n_A - (N_B - rF_B)/n_B}{(N_B - rF_B)/n_B}$, for model (1)
- $\rho_2 = \frac{N_A/F_A - N_B/F_B}{N_B/F_B}$, for model (2).

where, for e.g. population A : N_A is the total number of aftershocks (i.e., summed, not averaged, over all sequences in population A), F_A is the total number of pre-shocks, and n_A is the number of mainshocks. As F_A is intended to measure the background activity prior to the mainshock, hence before precursory acceleration, we here simply count the pre-shocks in the $-365 < t < -100$ interval. This conservative choice is done to avoid the $-30 < t < 0$ interval for which the acceleration is visually clear, see Figure 2. Coefficient r is then $r=365/265$, so that the product $r \cdot F_A$ gives the expected number of background earthquakes occurring in the 1 year after the mainshock. With both measures, $r > 0$ for a gain in productivity in population A compared to population B, and $r < 0$ in the opposite case.

We compute r_1 and r_2 for all 612 sequences, and smooth them over 100 sequences with neighboring values of p . Figure S4 demonstrates that the stronger productivity gains are obtained for low values of p , so that the observed relationship between precursory acceleration and the number of aftershocks is significant.

Dependence on location

We divide the Earth's surface into 14 regions for which the seismic activity allows to locally reproduce the analysis, see Figure 1. Most of the regions (with the exceptions of zones 3 and 6) correspond to subduction zones. We find that, out of these 14 regions, 9 exhibit the same behavior as the overall dataset, i.e., correlation of the number of aftershocks with the existence of a pre-mainshock acceleration (Figure S5), while 2 show an opposite relationship, see Figure S6. Of these two latter zones, one (Izu-Bonin) is dominated by one remarkably strong aftershock sequence ; discarding this sequence significantly affects this anti-correlation (Figure S6). The second zone showing the opposite relationship is North America; for this region, we note that 5 out the 6 mainshocks with precursory activity occur on oceanic transform faults, see Table S1. This type of earthquake is known to be preceded by intensive foreshock activity immediately prior to the

mainshock [McGuire, 2003], and to trigger relatively few aftershocks [McGuire et al., 2006; Boettcher and Jordan, 2004]. A recent well documented sequence occurring on the oceanic Gofar transform fault shows that accelerating creep prior to a M6.0 mainshock was halted by the main rupture, so that the transient deformation episode did not last past the end of the inter-seismic phase [McGuire et al., 2012], possibly due to partial draining of the high porosity barrier hosting the creep event. Such a mechanism, along with high thermal gradients, could explain why aftershock productivity is not enhanced by pre-seismic creep transients, although the lateral inhomogeneity in fault properties required by this model is perhaps specific to the Gofar fault system. 10 out of the 18 population B mainshocks for the North America region are also oceanic transform fault earthquakes (Table S2), but lack teleseismic $m \geq 4.0$ precursors.

We separately analyzed 26 other oceanic earthquakes related to spreading centers or transform faults, in the North and mid-Atlantic and in the Pacific oceans, that are not included in the regions boxed in Figure 1. Population A sequences have a greater aftershock production than population B sequences, see Figure S8, although the very low numbers of aftershocks overall is striking, partly due to detection biases for these sequences that are only observed teleseismically.

The negative correlation between foreshock and aftershock activities for North America is therefore due to the mixing of oceanic transform fault earthquakes together with other types of earthquakes (mainly continental): the former tend to have precursory activity more frequently but relatively fewer aftershocks than continental or subduction earthquakes, so that they form the bulk of population A earthquakes, but generate few aftershocks. Isolating oceanic earthquakes (Figure S8) allows to recover the ubiquitous, positive correlation between foreshock and aftershock activities.

Three zones display ambiguous behaviors, either as no significant departure between populations A and B is observed (region 12), or as we obtain different conclusions whether we apply our proposed correction for the difference in mainshock magnitude distributions between the two populations or not (regions 2 and 6).

References :

Boettcher M. S., and T. H. Jordan (2004), Earthquake scaling relations for mid-ocean ridge transform faults, *J. Geophys. Res.*, 109, B12302.

Marsan, D., and O. Lengliné (2008), Extending earthquakes' reach through cascading, *Science*, 319, 1076 – 1079.

McGuire J. J. (2003), Immediate foreshock sequences of oceanic transform earthquakes on the East Pacific Rise, *Bull. Seismol. Soc. Am.*, 93, 948-952.

McGuire J. J., J. A. Collins, P. Gouédard, E. Roland, D. Lizarralde, M. S. Boettcher, M. D. Behn, and R. D. Van der Hilst (2012), Variations in earthquake rupture properties along the Gofar transform fault, East Pacific Rise, *Nature Geosc.*, doi:10.1038.

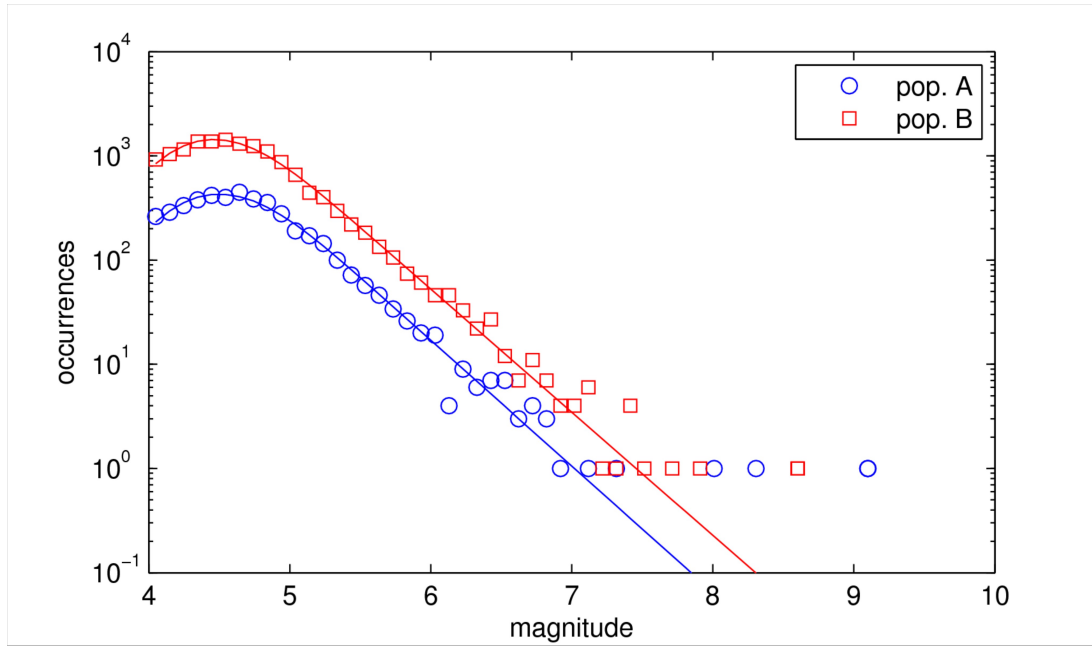


Figure S1. Number of occurrences vs magnitude for the aftershocks of populations A and B. The best fits obtained with a Gutenberg-Richter law modulated by an error function to account for incomplete detection at small magnitudes [Ogata and Katsura, 1993] are shown. The b-values are estimated to 1.21 ± 0.06 and 1.18 ± 0.03 for population A and B aftershocks, respectively.

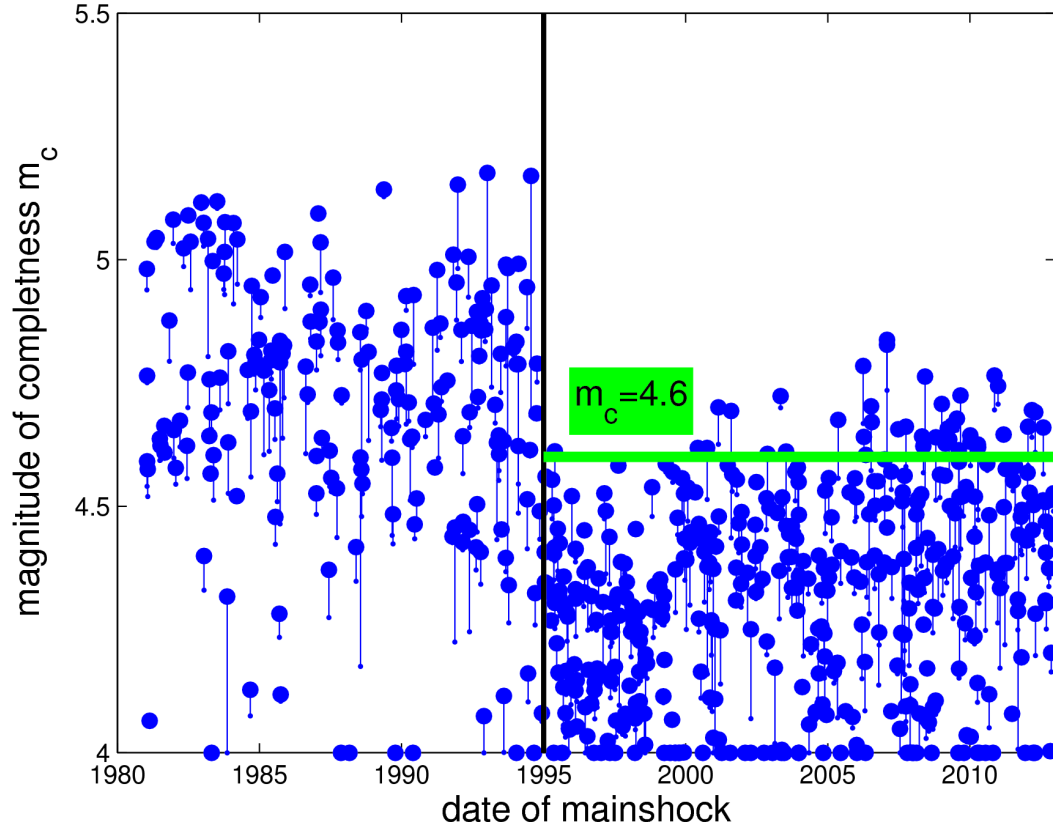


Figure S2. Magnitude of completeness m_c function of the date of the mainshock (big dots). It stabilizes from 1995 onwards to a value of 4.6 or less for 90% of the sequences. The vertical lines connect the two values of m_c estimated with $n_{\min}=100$ and $n_{\min}=200$. We define m_c as the maximum of these two values (big dots).

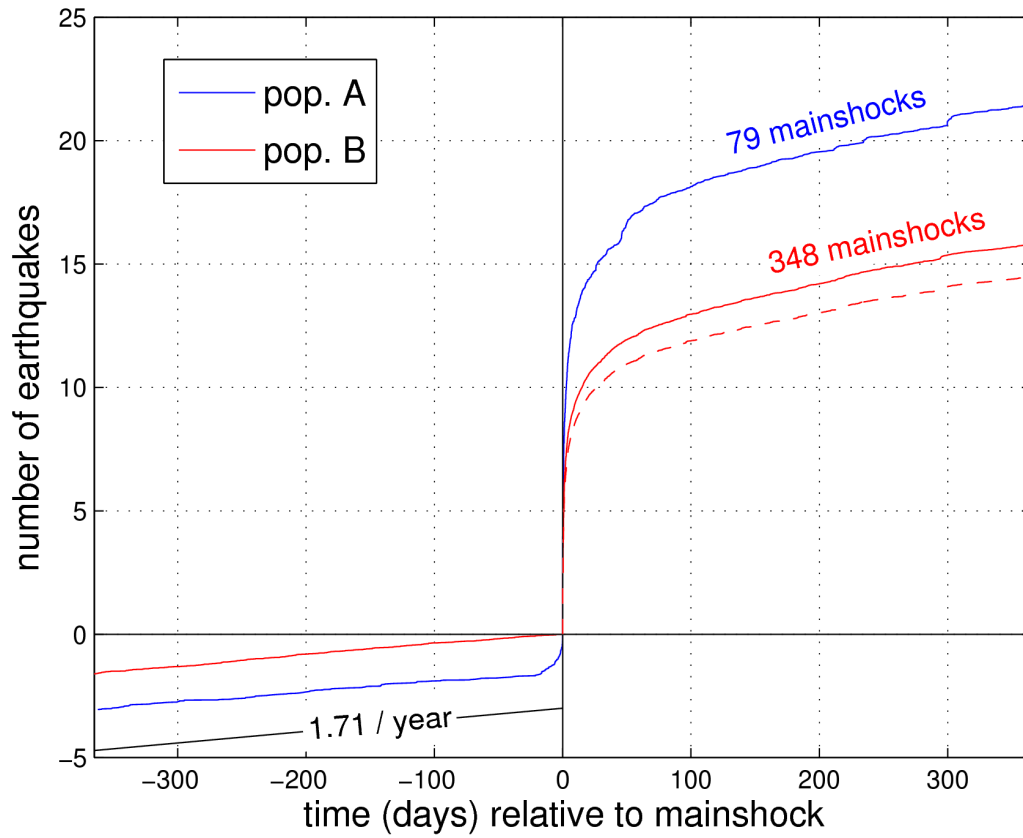


Figure S3. Identical to Figure 2, but only considering mainshocks occurring from 1995 onwards, and earthquakes of magnitude $m \geq 4.6$. The correction (dashed red curve) to the number of aftershocks in population B due to the fact that the two populations do not have the same distribution of mainshock magnitudes is based on the ratio $N_B/N_A = 1.09$ expected for a productivity law in $\exp(1.82 \cdot m)$.

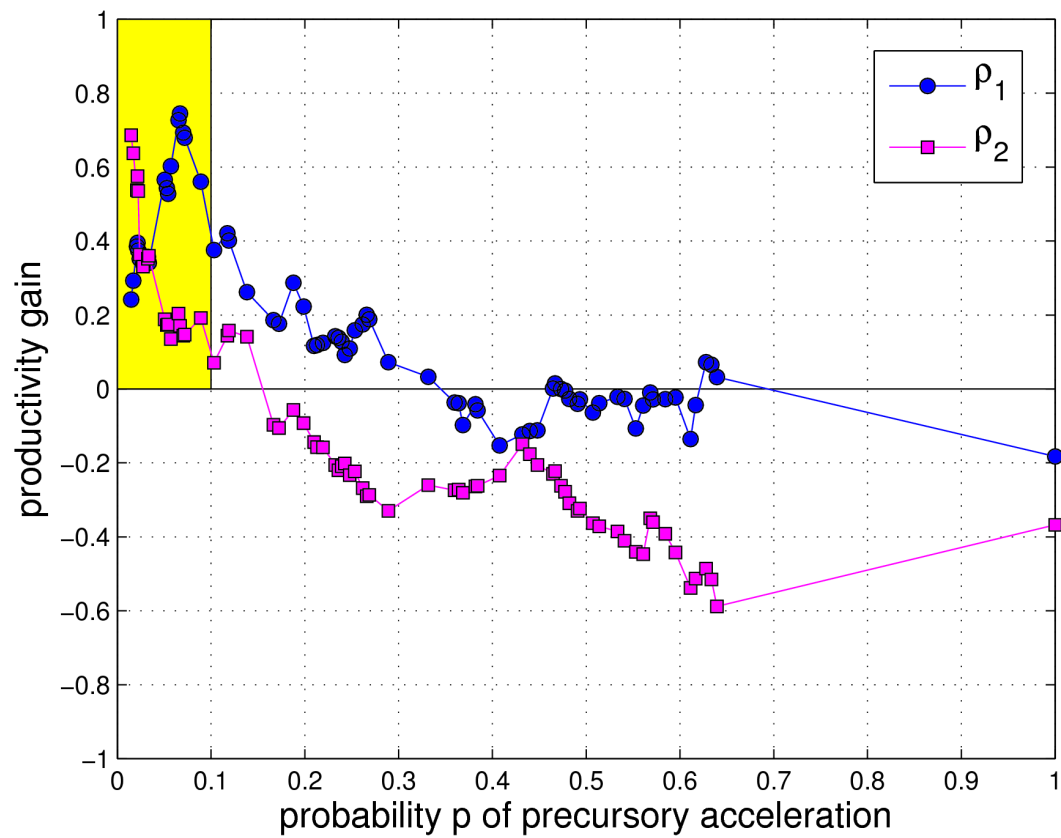


Figure S4. Two measures of the gain in aftershock productivity, function of p . Smoothing has been performed by averaging both the gains and the probabilities p over (overlapping) windows of 100 sequences with neighboring values of p . The $0 \leq p \leq 0.1$ window used in our analysis to select accelerating sequences is highlighted in yellow.

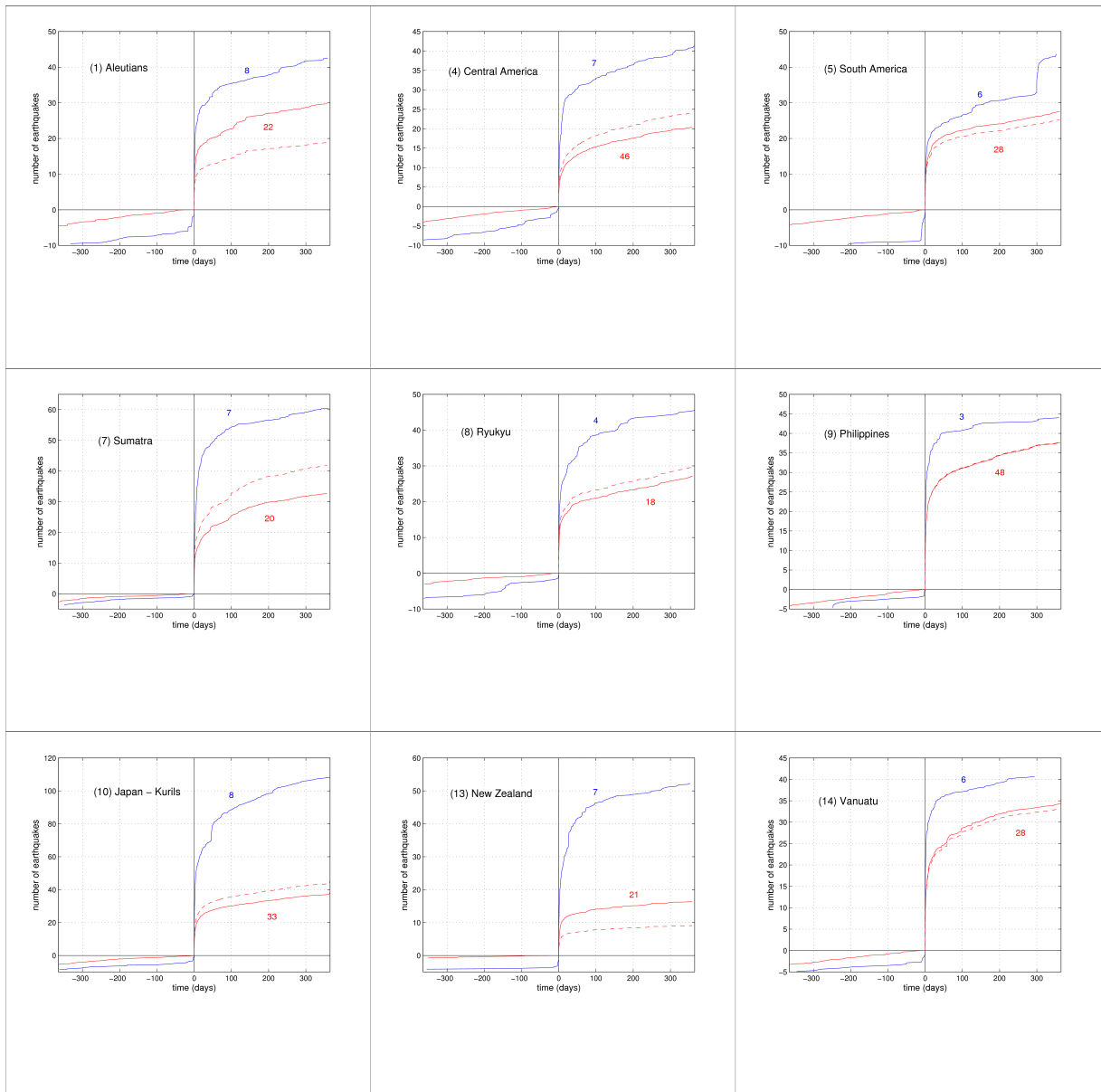


Figure S5. As in Figure 2, for the 9 regions that exhibit a positive correlation between the existence of an acceleration prior to the mainshock and the number of aftershocks. The red dashed line is corrected for the difference in mainshock magnitude distributions between the two populations.

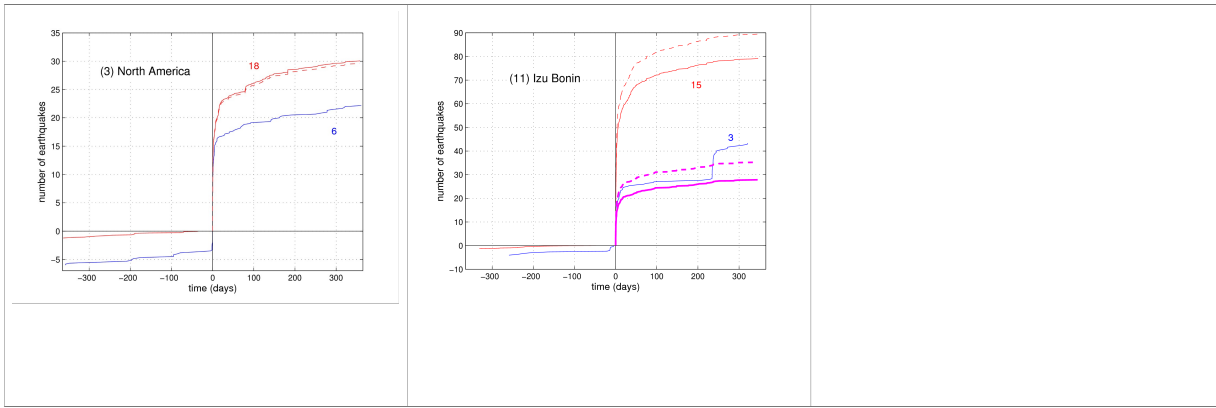


Figure S6. As in Figure S5, but for the two regions that show a negative correlation. The Izu-Bonin region is dominated in this analysis by the normal-faulting, M7.4, 21/12/2010 Bonin islands mainshock (ref USGS), which has the strongest aftershock sequence of all world-wide 612 mainshocks studied here, see Figure 3. Removing this sequence from this analysis gives the two thick magenta curves, that show an ambiguous correlation as observed for other zones (see Figure S7).

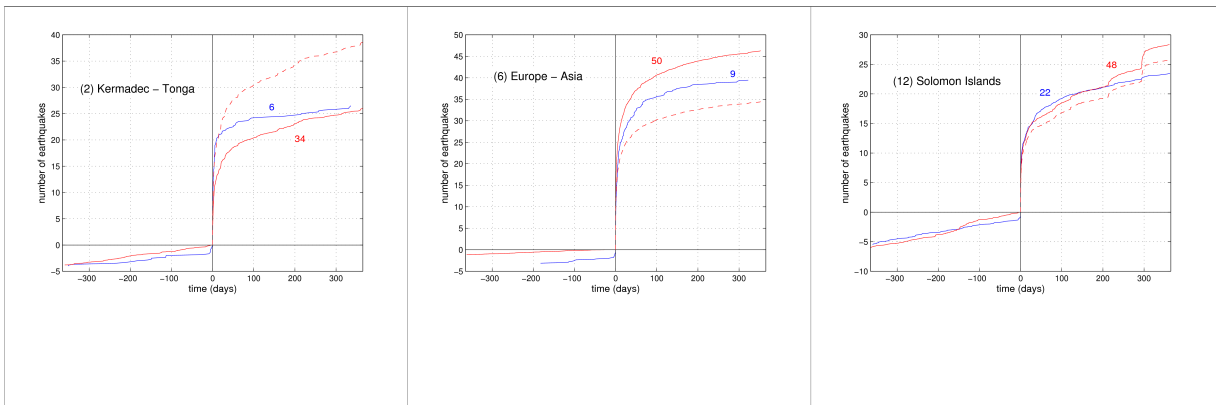


Figure S7. As in Figure S5, but for the three regions that show an ambiguous relationship.

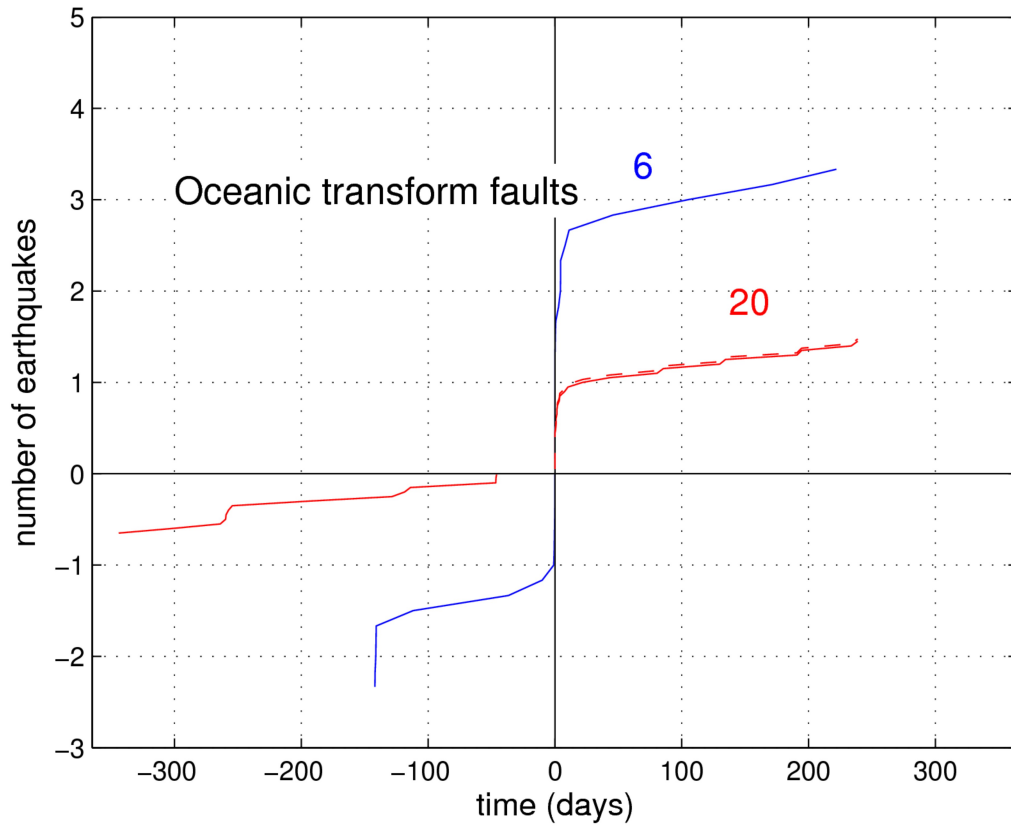


Figure S8. As in Figure S5, but for oceanic transform faults not included in the regions boxed in Figure 2.

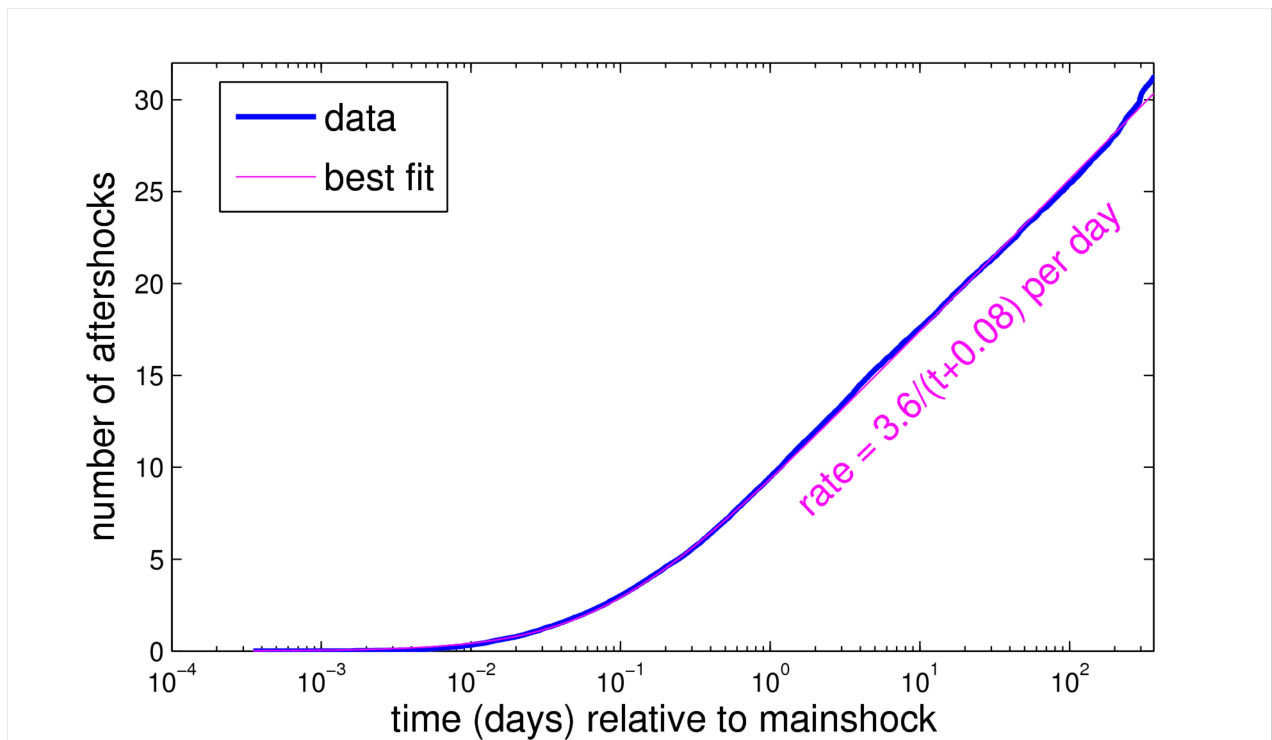


Figure S9. Number of aftershocks, averaged over the 612 sequences (i.e., not distinguishing the two populations A and B). The best fit gives a rate of $K/(t+c)$ with $K=3.6$ and $c=0.08$ days.

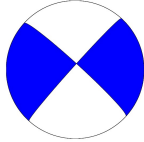
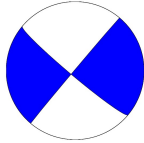
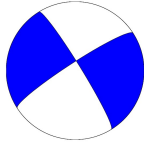
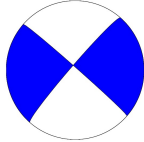
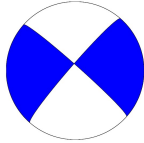
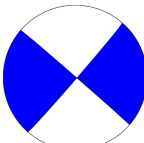
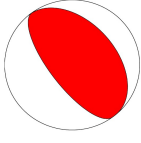
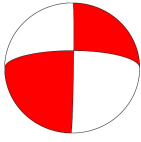
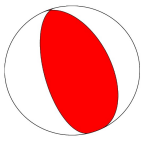
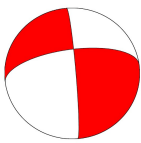
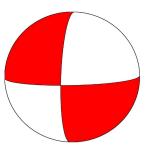
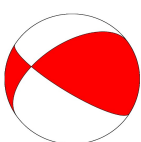
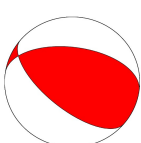
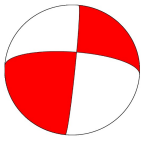
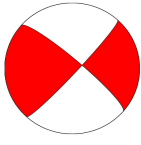
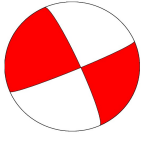
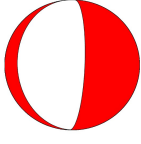
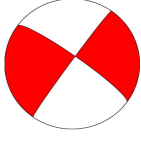
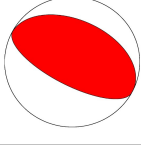
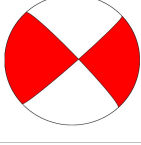
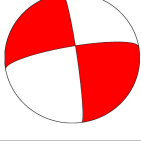
Date	Region	m	Z (km)	CMT focal mechanism	Comment	Nf / Na
2004/11/2	Near Vancouver Island	6.7	10		Oceanic transform fault earthquake	2 (2) / 21
2006/1/4	Gulf of California	6.6	14		Oceanic transform fault earthquake	4 (4) / 5
2008/1/5	Queen Charlotte Islands	6.6	10		Oceanic transform fault earthquake	5 (3) / 9
2009/8/3	Gulf of California	6.9	10		Oceanic transform fault earthquake	1 (1) / 3
2010/4/4	Sierra El Mayor	7.2	10		(USGS) « The April 4 main-shock occurred along a strike-slip segment of the plate boundary that coincides with the southeastern part of the Laguna Salada fault system »	12 (1) / 80
2010/10/21	Gulf of California	6.7	10		Oceanic transform fault earthquake	13 (3) / 15

Table S1. Characteristics of the 6 mainshocks in population A for the North America region. The region, magnitude and depth are taken from the USGS Significant Earthquake and News Headlines Archive. The number of $m \geq 4$ foreshocks (Nf) and aftershocks (Na) in the last column are for 1

year before / after the mainshock, and within 50 km of its epicenter. The number of immediate foreshocks, i.e., occurring in the 1 day prior to the mainshock and within 50 km, is given in parenthesis.

Date	Region	m	Z (km)	CMT focal mechanism	Comment	Nf / Na
1983/5/2	Coalinga earthquake	6.7	10		Continental	4 (0) / 42
1984/9/10	Northern California	6.6	4		Oceanic transform fault earthquake	5 (0) / 13
1985/10/5	North-West Canada	6.6	10		Continental	0 / 50
1987/11/17	Gulf of Alaska	6.6	10		Oceanic transform fault earthquake	0 / 49
1988/3/6	Gulf of Alaska	6.8	10		Oceanic transform fault earthquake	1 (0) / 31
1989/10/18	Loma Prieta earthquake	7.0	17		Continental	6 (0) / 56
1994/1/17	Northridge earthquake	6.7	18		Continental	0 / 52

1994/9/1	Northern California	7.0	10		Oceanic transform fault earthquake	1 (0) / 8
1995/8/28	Gulf of California	6.6	12		Oceanic transform fault earthquake	0 / 1
1999/10/16	Hector Mine earthquake	7.1	0		Continental	0 / 61
2001/2/28	Nisqually earthquake	6.8	51		Intra-slab earthquake	0 / 1
2002/10/3	Gulf of California	6.5	10		Oceanic transform fault earthquake	1 (0) / 0
2003/12/22	San Simeon earthquake	6.5	8		Continental	0 / 17
2005/6/15	Northern California	7.2	16		Oceanic transform fault earthquake	1 (0) / 10
2009/11/17	Queen Charlotte Islands	6.6	17		Oceanic transform fault earthquake	2 (0) / 5

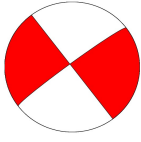
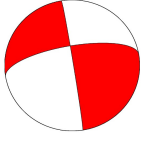
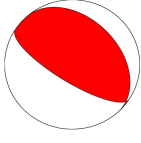
2010/1/10	Northern California	6.5	29		Oceanic transform fault earthquake	2 (0) / 7
2011/9/9	Vancouver Island	6.5	22		Oceanic transform fault earthquake	0 / 1
2012/10/28	Queen Charlotte Islands	7.8	14		Thrust oceanic crustal earthquake	0 / 138

Table S2. Same as Table S1, for population B mainshocks in the North America region. Depth is from the ANSS catalog.